



HAL
open science

Macro-scale numerical investigation of the contribution of Van der Waals force to the pressure-drop overshoot in fine-particle fluidized beds

Youssef Badran, Renaud Ansart, Jamal Chaouki, Olivier Simonin

► To cite this version:

Youssef Badran, Renaud Ansart, Jamal Chaouki, Olivier Simonin. Macro-scale numerical investigation of the contribution of Van der Waals force to the pressure-drop overshoot in fine-particle fluidized beds. Powder Technology, 2024, 436, pp.119505. 10.1016/j.powtec.2024.119505 . hal-04524470

HAL Id: hal-04524470

<https://hal.science/hal-04524470>

Submitted on 28 Mar 2024

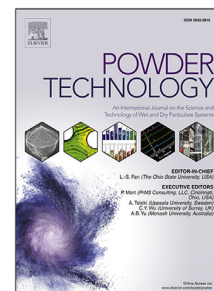
HAL is a multi-disciplinary open access archive for the deposit and dissemination of scientific research documents, whether they are published or not. The documents may come from teaching and research institutions in France or abroad, or from public or private research centers.

L'archive ouverte pluridisciplinaire **HAL**, est destinée au dépôt et à la diffusion de documents scientifiques de niveau recherche, publiés ou non, émanant des établissements d'enseignement et de recherche français ou étrangers, des laboratoires publics ou privés.

Journal Pre-proof

Macro-scale numerical investigation of the contribution of Van der Waals force to the pressure-drop overshoot in fine-particle fluidized beds

Youssef Badran, Renaud Ansart, Jamal Chaouki, Olivier Simonin



PII: S0032-5910(24)00147-5

DOI: <https://doi.org/10.1016/j.powtec.2024.119505>

Reference: PTEC 119505

To appear in: *Powder Technology*

Received date: 7 November 2023

Revised date: 4 January 2024

Accepted date: 4 February 2024

Please cite this article as: Y. Badran, R. Ansart, J. Chaouki et al., Macro-scale numerical investigation of the contribution of Van der Waals force to the pressure-drop overshoot in fine-particle fluidized beds, *Powder Technology* (2024), doi: <https://doi.org/10.1016/j.powtec.2024.119505>.

This is a PDF file of an article that has undergone enhancements after acceptance, such as the addition of a cover page and metadata, and formatting for readability, but it is not yet the definitive version of record. This version will undergo additional copyediting, typesetting and review before it is published in its final form, but we are providing this version to give early visibility of the article. Please note that, during the production process, errors may be discovered which could affect the content, and all legal disclaimers that apply to the journal pertain.

© 2024 Published by Elsevier B.V.

Macro-scale numerical investigation of the contribution of Van der Waals force to the pressure-drop overshoot in fine-particle fluidized beds

Youssef BADRAN^{a,b}, Renaud ANSART^a, Jamal CHAOUKI^b, Olivier SIMONIN^{c,*}

^a*Laboratoire de Génie Chimique, Université de Toulouse, CNRS, INPT, UPS, Toulouse, France*

^b*Department of Chemical Engineering, Polytechnique Montréal, P.O. Box 6079, Station Centre-ville, Montréal, Québec H3C 3A7, Canada*

^c*Institut de Mécanique des Fluides de Toulouse (IMFT), Université de Toulouse, CNRS, Toulouse, France*

Abstract

Interparticle Van der Waals force contributes to the overshoot in the bed pressure drop at the minimum fluidization velocity during the transition from static to fluidized bed conditions, which is a well-known phenomenon in the fluidization of fine particles. In this study, two adhesive particle pressure closures considering the effect of interparticle Van der Waals force are used in two-fluid model simulations with the intention to generate the pressure overshoot. The first adhesive pressure model developed within the context of the kinetic theory of rapid granular flows failed to produce the overshoot due to the dominance of multiple and long duration contacts in the fixed-bed flow. Another closure based on the coordination number was then proposed to represent long-lasting interparticle contacts, which gave an adhesive con-

*Corresponding author

Email address: olivier.simonin@toulouse-inp.fr (Olivier SIMONIN)

tribution much larger than the one of the kinetic theory model and was able to create the pressure drop overshoot.

Keywords: Gas-solid fluidized beds, Interparticle forces, Van der Waals adhesion, Granular media, Two-fluid model, Kinetic theory

1. Introduction

Gas-solid fluidized beds are employed in several industries, such as the polymerization of olefins, fluid catalytic cracking (FCC), coal combustion, and ore roasting [1]. Good quality solids mixing, high rates of mass and heat transfer, uniform temperature distribution, and the capability of processing a broad variety of granular materials are among the features of fluidized-bed reactors [1, 2, 3, 4, 5]. Interparticle forces, such as Van der Waals, electrostatic, liquid bridge, and solid bridge forces, may have a significant influence on fluidized bed hydrodynamics and performance [6, 7, 8, 9, 10, 11, 12].

Fine particles ranging from cohesive to aeratable are highly desirable for reactive fluidization processes due to their high surface-to-volume ratio, which results in greater reaction rates per unit volume of reactor [13]. The pressure drop overshoot at the minimum fluidization velocity is a typically encountered phenomenon in beds of fine particles belonging to the group A of Geldart's classification [14]. A more intense overshoot and a larger hysteresis area between the fluidization and defluidization pressure-drop curves are observed upon decreasing the particle diameter towards Geldart's C group [15]. This observation is owing to the dominant role of interparticle over hydrodynamic interactions in static beds of these particles. The Van der Waals

21 adhesive force is the dominating interaction force between fine particles in a
22 dry ambient environment [16].

23 Van der Waals forces include dipole-dipole, dipole-induced dipole, and in-
24 stantaneous dipole-induced dipole forces acting between atoms and molecules.
25 The temporal average of a neutral atom's dipole moment is zero, yet at ev-
26 ery instant there is a definite polar moment provided by the asymmetrical
27 electron distribution around the protons that are inside the nucleus [17].
28 This instantaneous dipole produces an electric field, which creates a dipole
29 moment in any adjacent neutral atom [17]. The two dipoles then interact,
30 resulting in a force of attraction among the two atoms. The temporal average
31 of this instantaneous dipole-induced dipole force, which is also known as the
32 London dispersion force, is finite. Hamaker [18] obtained an expression for
33 the Van der Waals force between macroscopic objects using the dispersion
34 interaction potential between two atoms/molecules proposed by London [19]
35 and an additivity hypothesis (summing up the forces over all pairs of individ-
36 ual atoms/molecules). The Van der Waals force between particles in contact
37 is highly influenced by their surface roughness (i.e., asperity size) [20, 21].

38 Working at high temperatures and/or high pressures has an impact on
39 the strength of Van der Waals force. The Van der Waals force increases with
40 temperature due to greater molecular dipole pulsation and a larger particle-
41 particle contact area induced by viscoelastic flattening [22, 23, 24, 21]. The
42 magnitude of the Van der Waals force can rise with pressure owing to gas
43 adsorption on the particle surfaces [25, 26, 4]. It is worth mentioning that
44 hydrodynamic forces can increase dramatically with pressure (gas density
45 increases with pressure), which may result in a less prominent influence of

46 interparticle interactions on the bed hydrodynamics [4].

47 Stresses caused by adhesive and frictional interactions have a signifi-
48 cant influence on the mechanical response of granular media [27]. There
49 is, however, insufficient data on the magnitude of these stresses, which limits
50 comprehension of the fluidization behavior reported in experimental studies.
51 Mutsers and Rietema [28] and Tsinontides and Jackson [29] postulated that
52 the interparticle contact adhesion and friction are responsible for the stable
53 expansion occurring between the minimum fluidization and minimum bub-
54 bling velocities in fine-particle beds. Rietema and Piepers [30] ascribed the
55 pressure drop overshoot at incipient fluidization to interparticle and particle-
56 wall forces. According to these authors, the Van der Waals interaction is the
57 source of particle-particle force. The non-sphericity can enhance the solid
58 friction and the pressure-drop hysteresis [31, 32, 33, 34].

59 In the experiments carried out by Vanni et al. [32], the static wall friction
60 effect on the pressure overshoot was only noticeable in columns with small
61 diameters ($D = 2$ cm). The experiments of Srivastava and Sundaresan [27]
62 also revealed a more significant overshoot in smaller columns, which they
63 ascribed to particle-wall friction. Wang et al. [35] observed that increasing
64 the static bed height increases the pressure overshoot intensity, which they
65 attributed to wall friction. The effect of bed diameter and height on the
66 significance of static wall friction (bridging) can also be seen in the vertical
67 solid stress profiles showing the Janssen effect in silos and hoppers [36, 37].

68 Several researchers accounted for the Van der Waals force in the Eulerian-
69 Lagrangian model to simulate the fluidization behavior of fine particles. Ho
70 and Sommerfeld [38] used a criterion for agglomeration based on a critical

71 velocity determined from an energy conservation between before and after
72 collision that takes into account the Van der Waals force. These authors
73 considered that when the normal relative velocity between two interacting
74 particles is smaller than the critical velocity, agglomeration occurs. Wang et
75 al. [39] solved a Newtonian equation of motion with a Van der Waals force
76 term based on the Hamaker theory for each particle in a fluidized bed riser.
77 Zhang et al. [40] investigated the cluster dynamics in circulating fluidized-
78 bed reactors using a CFD-DEM model. Their simulations showed that when
79 the solid volume fraction α_p is large, the Van der Waals interaction may
80 promote the cluster formation.

81 On the other hand, Eulerian-Eulerian models that take into considera-
82 tion the impact of interparticle Van der Waals interaction are scarce in the
83 literature. Within the framework of the kinetic theory of granular flows,
84 Gidaspow and Huilin [41] added a negative pressure inferred from the exper-
85 imental data of radial distribution functions to the solid pressure in order
86 to consider the effect of adhesive forces on the fluidization of FCC parti-
87 cles. This empirical adhesive pressure modified the kinetic theory equation
88 of state to match the measured particle pressure. Parmentier [42] worked on
89 incorporating the effect of Van der Waals interaction into the two-fluid model
90 utilizing the BBGKY hierarchy. An adhesive pressure was added to the par-
91 ticle pressure to account for the Van der Waals attraction between particles.
92 By comparing the magnitudes of attractive and repulsive solids pressures
93 within a bed of Geldart A particles in the fluidized state (small attraction),
94 Parmentier [42] concluded that the overestimation of bed expansion found
95 in standard two-fluid model simulations is not due to neglecting the effect

96 of the Van der Waals force. The kinetic theory based on the assumptions
97 of binary collision and molecular chaos may be extended from moderately
98 dense to highly dense gas-solid flows by utilizing numerical data of discrete
99 element simulations [43, 44, 45].

100 Some efforts have been made to predict the pressure-drop overshoot phe-
101 nomenon observed during the fluidization of fine particles. Srivastava and
102 Sundaresan [27] and Loezos et al. [46] utilized a one-dimensional force bal-
103 ance model based on Janssen's approach in order to predict the pressure drop
104 overshoot. This model involves determining coefficients that can combine the
105 adhesion and friction effects together. For instance, when the particle diam-
106 eter decreases, the friction coefficient of Loezos et al. [46] increases, which
107 may be attributed to an increase in the significance of the Van der Waals
108 adhesive interaction. Ye et al. [47] demonstrated through discrete particle
109 simulations that the pressure overshoot is caused by particle-particle Van der
110 Waals adhesion and particle-wall friction. Weber and Hrenya [48] conducted
111 discrete particle simulations employing Hamaker and square-well adhesion
112 models. Their findings reveal that the overshoot in the bed pressure drop
113 is dominated by interparticle adhesion. The Hamaker model predicted that
114 Van der Waals adhesive interactions with the sidewalls have a considerable
115 impact on the pressure-drop overshoot (adhesion augments wall friction),
116 whereas adhesive interactions with the distributor plate have minimal im-
117 pact. The square-well model, on the other hand, predicted that particle-
118 distributor plate adhesion has a considerable influence on the pressure-drop
119 overshoot.

120 Interparticle adhesive forces affect both solid pressure and viscosity (nor-

mal and shear stresses) [49, 50, 51]. The influence of particle viscosity on the pressure overshoot, which is associated with a fixed arrangement of particles (zero particle velocity), is negligible. Hence, we consider only the effect of adhesion on the solid pressure. In our investigation, we take into account the short-range Van der Waals interaction between particles via an adhesive pressure gradient in the particle momentum equation within an Eulerian-Eulerian approach. We present two adhesive pressure models, one based on the kinetic theory and another based on the coordination number to represent interparticle contacts, and assess their capability of creating a pressure-drop overshoot in beds of Geldart A particles.

2. Prediction of overshoot in pressure drop across an aeratable-particle bed

Soleimani et al. [14] performed experimental measurements of the total bed pressure drop and bed voidage of Geldart A and Geldart B particles fluidized by air at 20 °C. The air was pre-dried by passing it through a bed of humidity adsorber. As a result, capillary forces have a negligible effect. The properties of the solids used in their study are shown in Table 1. The experiments were carried out in a fluidized bed of 5.25 cm in diameter and 50 cm in height. The static bed height was around 15 cm. For details about the procedure employed to determine the experimental bed pressure drop and voidage, the reader is referred to the paper of Soleimani et al. [14].

Table 1

Properties of particles used in the experiments of Soleimani et al. [14].

Material	Glass beads	Glass beads
Mean particle diameter, d_p (μm)	156	67
Particle density, ρ_p (kg/m^3)	2595	2595
Sphericity	~ 1	~ 1
Geldart group	B	A
Acronym	GB-156	GB-67

142 The experimental bed pressure drop and voidage profiles as a function of
 143 the superficial gas velocity of the Geldart B and A glass beads determined
 144 by Soleimani et al. [14] are demonstrated in Fig. 1. It can be seen that the
 145 increasing velocity path pressure drop curve of the Geldart B particles has
 146 no overshoot since the associated loose-fixed-bed and minimum fluidization
 147 voidages (ε_0 and ε_{mf} , respectively) are nearly equal. In contrast, a consider-
 148 able pressure drop overshoot is apparent at the minimum fluidization velocity
 149 (U_{mf}) in the fluidization branch of the experiment with Geldart A particles,
 150 which is equivalent to the difference between the fixed-bed and minimum
 151 fluidization voidages.

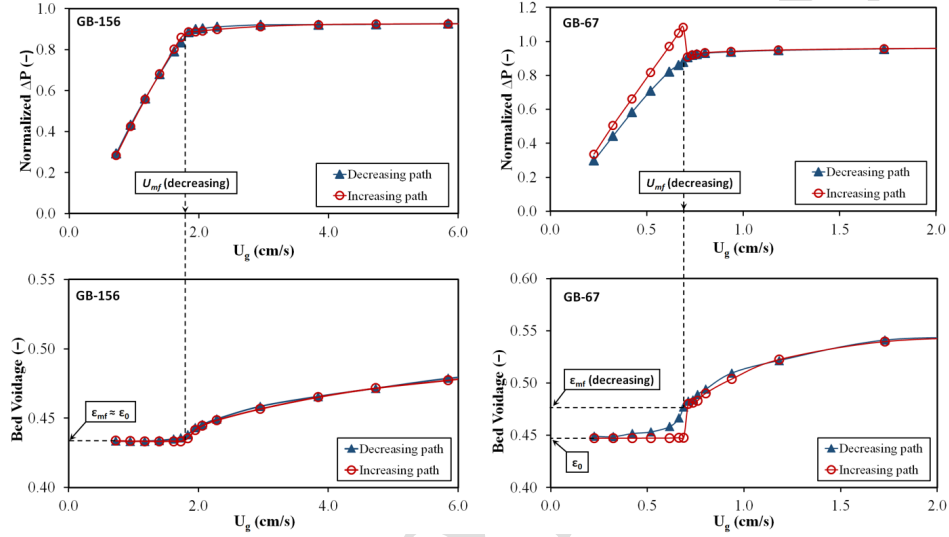


Fig. 1. Normalized bed pressure drop and corresponding voidage profiles of Geldart B (GB-156) and A (GB-67) particles measured by Soleimani et al. [14].

152 In our study, we perform two-fluid simulations using the `neptune.cfd` code
 153 [52]. Transport equations and models employed in this code are reported in
 154 Ansart et al. [53]. The particle stress in the Eulerian-Eulerian model consists
 155 of kinetic, collisional and frictional terms. The closure of the kinetic and
 156 collisional stresses is based on the kinetic theory of granular flows. In dilute
 157 flows ($\alpha_p < 1\%$), the kinetic stress is dominant, whereas in moderately dense
 158 flows ($\alpha_p > 5\%$), the collisional stress dominates. The particle friction stress
 159 is employed at high solid volume fractions to take into account the interaction
 160 of single particles with several neighbors through prolonged contact. The
 161 normal particle-particle forces are considered via the particle pressure [54].
 162 For the particle frictional pressure, we have employed the following semi-

163 empirical model proposed by Johnson and Jackson [55, 56]:

$$P_p^f = \begin{cases} Fr \frac{(\alpha_p - \alpha_{p,min})^n}{(\alpha_{p,max} - \alpha_p)^m} & \text{for } \alpha_p > \alpha_{p,min} \\ 0 & \text{for } \alpha_p \leq \alpha_{p,min} \end{cases} \quad (1)$$

164 where Fr , n and m are constants and $\alpha_{p,min}$ and $\alpha_{p,max}$ are respectively
 165 the threshold particle volume fraction for the activation of the frictional
 166 stress and the close-packing particle volume fraction. The values of these
 167 parameters used in our simulations are listed in Table 2. To account for the
 168 Van der Waals interaction among particles, a negative adhesive pressure is
 169 added to the particle pressure for all values of the particle volume fraction
 170 α_p in our work. The additional negative stress component has the effect
 171 of lowering particle repulsion. In the following sections, we propose two
 172 adhesive pressure models and investigate their ability to create a pressure
 173 drop overshoot.

174 2.1. Derivation of an adhesive pressure model based on the kinetic theory

The kinetic theory approach relies on the similarity between the random particle movement in rapid granular flow and the thermal motion of molecules in gas [57]. The adhesive pressure model derivation employing the kinetic theory of granular flows given in this subsection is based on the research of Parmentier [42]. Using the BBGKY hierarchy, the Van der Waals force can be included in the Boltzmann-Liouville equation:

$$\begin{aligned} \frac{\partial f_p}{\partial t} + \frac{\partial}{\partial x_i} (c_{p,i} f_p) + \frac{\partial}{\partial c_{p,i}} \left(\left\langle \frac{F_{p,i}}{m_p} \mid \mathbf{x}_p = \mathbf{x}, \mathbf{u}_p = \mathbf{c}_p \right\rangle f_p \right) \\ = \left(\frac{\partial f_p}{\partial t} \right)_{coll} + \left(\frac{\partial f_p}{\partial t} \right)_{ad} \end{aligned} \quad (2)$$

175 with [58]

$$\left(\frac{\partial f_p}{\partial t}\right)_{ad} = \iint \frac{\partial f_p^{(2)}}{\partial c_{p,i}} \frac{\partial}{\partial x_i} \left(\frac{V(\|\mathbf{x}^* - \mathbf{x}\|)}{m_p} \right) d\mathbf{c}_p^* d\mathbf{x}^* \quad (3)$$

176 where f_p is the one-particle probability density function defined such that
 177 $f_p(\mathbf{c}_p, \mathbf{x}, t) \delta\mathbf{c}_p \delta\mathbf{x}$ is the probable number of particles, whose center of mass,
 178 \mathbf{x}_p , at time t is located in the volume $[\mathbf{x}, \mathbf{x} + \delta\mathbf{x}]$ with a velocity \mathbf{u}_p in
 179 $[\mathbf{c}_p, \mathbf{c}_p + \delta\mathbf{c}_p]$. $F_{p,i}$ represents the external forces acting on the particles
 180 (gravity, drag and buoyancy). $F_{p,i}/m_p = du_{p,i}/dt$ is the acceleration of a
 181 particle. $\langle F_{p,i} | \mathbf{x}_p = \mathbf{x}, \mathbf{u}_p = \mathbf{c}_p \rangle$ represents the conditional average of the
 182 external force acting on a particle at a given center position $\mathbf{x}_p = \mathbf{x}$ with
 183 the translation velocity $\mathbf{u}_p = \mathbf{c}_p$. The two terms on the right-hand side
 184 of Eq. (2) denote the rate of change in the probability density function
 185 caused by particle-particle collision and Van der Waals adhesion, respectively.
 186 The adhesion term is given by Eq. (3), where $f_p^{(2)}(\mathbf{c}_p, \mathbf{x}, \mathbf{c}_p^*, \mathbf{x}^*, t)$ is the
 187 two-particle probability density function and $V(\|\mathbf{x}^* - \mathbf{x}\|)$ is the interaction
 188 potential between two particles resulting in an adhesion force. According to
 189 Elimelech et al. [59], the Van der Waals interaction potential between two
 190 spheres can be expressed as follows:

$$V(\|\mathbf{x}^* - \mathbf{x}\|) = -\frac{A}{24} \left[\frac{2}{2u + u^2} + \frac{2}{(1 + u)^2} + 4 \ln \left(\frac{2u + u^2}{[1 + u]^2} \right) \right] \quad (4)$$

191 where $u = \|\mathbf{x}^* - \mathbf{x}\|/d_p - 1$ is the dimensionless distance between the two
 192 particle surfaces and A is the Hamaker constant, which relies on the compo-
 193 sition of the particles and the interstitial fluid. The adhesive force exerted
 194 by particle p^* , with its center at \mathbf{x}^* , on particle p , with its center at \mathbf{x} , as a
 195 result of the Van der Waals potential given by Eq. (4) can be written as:

$$\mathbf{F}_{p^* \rightarrow p}^{ad} = \frac{A}{6d_p} \frac{1}{(2u + u^2)^2} \frac{1}{(1 + u)^3} \frac{\mathbf{x}^* - \mathbf{x}}{\|\mathbf{x}^* - \mathbf{x}\|} \quad (5)$$

196 For distances between the surfaces of two particles less than a typical in-
 197 teratomic distance S_0 , Eqs. (4) and (5) are no longer applicable and the
 198 magnitude of the Van der Waals force is fixed at a maximal value in order
 199 to represent the physical particle-particle repulsion and prevent the single
 200 attraction when the surface separation distance is zero [60].

201 Assuming that the velocities of colliding particles are not correlated (En-
 202 skog approximation for dense flows), the two-particle probability density
 203 function is defined as follows:

$$f_p^{(2)}(\mathbf{c}_p, \mathbf{x}, \mathbf{c}_p^*, \mathbf{x}^*, t) = g(\mathbf{x}, \mathbf{x}^*) f_p(\mathbf{c}_p, \mathbf{x}, t) f_p(\mathbf{c}_p^*, \mathbf{x}^*, t) \quad (6)$$

204 with $g(\mathbf{x}, \mathbf{x}^*)$ being the two-particle radial distribution function. The adhe-
 205 sion term in Eq. (3) can then be written as:

$$\left(\frac{\partial f_p}{\partial t}\right)_{ad} = -\frac{\partial}{\partial c_{p,i}} \left(\frac{F_{a,i}}{m_p} f_p\right) - \frac{\partial}{\partial c_{p,i}} \left(\frac{F_{b,i}}{m_p} f_p\right) \quad (7)$$

206 with

$$F_{a,i} = -\frac{\partial}{\partial x_i} \int n_p(\mathbf{x}^*) g(\mathbf{x}, \mathbf{x}^*) V(\|\mathbf{x}^* - \mathbf{x}\|) d\mathbf{x}^* \quad (8)$$

207

$$F_{b,i} = \int n_p(\mathbf{x}^*) \frac{\partial g(\mathbf{x}, \mathbf{x}^*)}{\partial x_i} V(\|\mathbf{x}^* - \mathbf{x}\|) d\mathbf{x}^* \quad (9)$$

208 where n_p is the particle number density. $F_{a,i}$ and $F_{b,i}$ can be approximated
 209 as follows:

$$F_{a,i} \approx -\frac{\partial}{\partial x_i} n_p(\mathbf{x}) g_0(\mathbf{x}) \int V(\|\mathbf{x}^* - \mathbf{x}\|) d\mathbf{x}^* \quad (10)$$

210

$$F_{b,i} \approx 0 \quad (11)$$

where g_0 is the radial distribution function at contact. A momentum balance equation for the solid phase containing a gradient of adhesive particle pressure

can then be derived from the Boltzmann-Liouville equation (Eq. (2)):

$$\alpha_p \rho_p \frac{\partial U_{p,i}}{\partial t} + \alpha_p \rho_p U_{p,j} \frac{\partial U_{p,i}}{\partial x_j} = -\alpha_p \frac{\partial P_g}{\partial x_i} + \alpha_p \rho_p g_i + I_{g \rightarrow p,i} - \frac{\partial}{\partial x_j} (\alpha_p \rho_p R_{p,ij} + \Theta_{p,ij}) - \alpha_p \frac{\partial P_{ad}}{\partial x_i} \quad (12)$$

211 where $I_{g \rightarrow p,i}$ is the mean interphase gas-to-particle momentum transfer and
 212 $R_{p,ij}$ and $\Theta_{p,ij}$ are respectively the particle kinetic and collisional stress ten-
 213 sors. Eq. (12) is derived by substituting (7) in (2) and then multiplying (2)
 214 by $m_p \mathbf{c}_p$ and integrating over all velocities \mathbf{c}_p . In Eq. (12), $-\alpha_p \partial P_{ad} / \partial x_i$
 215 is equal to $n_p F_{a,i}$, where $F_{a,i}$ is expressed by Eq. (10). P_{ad} represents an
 216 adhesive pressure resulting from the attraction between particles, which is
 217 given by:

$$P_{ad} \approx \frac{n_p g_0}{\pi d_p^3 / 6} \int V(\|\mathbf{x}^* - \mathbf{x}\|) d\mathbf{x}^* \quad (13)$$

218 In the case of Van der Waals interaction potential, P_{ad} may be written as:

$$P_{ad} \approx \frac{n_p g_0}{\pi d_p^3 / 6} \int_{\|\mathbf{x}^* - \mathbf{x}\| > d_p + S_0} V(\|\mathbf{x}^* - \mathbf{x}\|) d\mathbf{x}^* \quad (14)$$

219 And according to Parmentier [42]:

$$P_{ad} \approx -A n_p g_0 \ln \left(\frac{d_p}{S_0} \right) \quad (15)$$

220 The adhesion term in the momentum equation (Eq. (12)) is written as:

$$-\alpha_p \frac{\partial P_{ad}}{\partial x_i} = -\frac{\partial P_p^a}{\partial x_i} \quad (16)$$

221 with

$$P_p^a \approx -A \frac{n_p}{\alpha_p} \ln \left(\frac{d_p}{S_0} \right) \int_0^{\alpha_p} \alpha_p \left(g_0 + \alpha_p \frac{\partial g_0}{\partial \alpha_p} \right) d\alpha_p \quad (17)$$

222 The radial distribution function, g_0 , which may be viewed as a measure for
 223 the likelihood of particle-particle collision, is given as the following expression
 224 [61]:

$$g_0 = \left(1 - \frac{\alpha_p}{\alpha_{p,max}}\right)^{-2.5\alpha_{p,max}} \quad (18)$$

225 Using Eq. (17), the negative adhesive pressure can then be formulated as:

$$P_p^a = -\frac{B}{d_p^3} 2\alpha_{p,max}^2 \left[\frac{25}{6} + \left(-\frac{3}{2} \frac{\alpha_p^2}{\alpha_{p,max}^2} + \frac{20}{3} \frac{\alpha_p}{\alpha_{p,max}} - \frac{25}{6} \right) g_0 \right] \quad (19)$$

226 with

$$B = A \frac{3}{\pi} \ln \left(\frac{d_p}{S_0} \right) \quad (20)$$

227 where d_p is the particle diameter, α_p is the solid volume fraction, A is the
 228 Hamaker constant, and S_0 is a minimum cutoff separation distance between
 229 two particle surfaces. The adhesive pressure P_p^a given by Eq. (19) is added
 230 to the kinetic, collisional, and frictional pressures.

231 2.2. Evaluation of the kinetic-theory-based adhesion model

232 The adhesive pressure model presented in Eq. (19) is tested by adding
 233 it to the solids pressure and performing two-fluid model simulations similar
 234 to CFD-DEM simulations carried out by Hou et al. [62]. The values of the
 235 parameters used in our quasi-two-dimensional fluidized bed simulations of
 236 Geldart A particles are summarized in Table 2. The value of the initial solid
 237 volume fraction ($\alpha_{p,ini} = 0.6$) is chosen to be the same as that obtained from
 238 the CFD-DEM simulations of Hou et al. [62] for the fixed bed. The bottom
 239 face of the cuboid bed employed in our simulations acts as an inlet for gas
 240 and a wall with a no-slip condition for particles. The top face serves as a
 241 free outlet for both gas and solid phases with an imposed gauge pressure of

242 zero. The left and right faces (normal to the x-axis) are walls for both phases
 243 with a no-slip condition for each phase. A symmetry boundary condition is
 244 employed for both phases at the front and back faces (normal to the y-axis).

Table 2

Simulation parameters.

Parameter	Value
Particle diameter, d_p	100 μm
Particle density, ρ_p	1440 kg/m^3
Particle-particle normal restitution coefficient, e_c	0.8
Gas density, ρ_g	1.205 kg/m^3
Gas viscosity, μ_g	1.8×10^{-5} Pa.s
Cuboid bed size, $L_x \times L_y \times L_z$	$60d_p \times 4d_p \times 200d_p$
Cell size, $\Delta x = \Delta y = \Delta z$	$2d_p$
Initial particle bed height, H_{ini}	$36d_p$
Initial particle volume fraction, $\alpha_{p,ini}$	0.6
Frictional pressure constant (Eq. (1)), Fr	0.05 Pa
Frictional pressure constant (Eq. (1)), n	2
Frictional pressure constant (Eq. (1)), m	5
Threshold solid volume fraction for friction, $\alpha_{p,min}$	0.58
Close-packing solid volume fraction, $\alpha_{p,max}$	0.64
Minimum surface separation distance, S_0	1 nm
Base value of the Hamaker constant, A	2.1×10^{-21} J
Maximum Courant number, CFL_{max}	0.1

245 The equations for the kinetic, collisional and frictional solids stress clo-

246 sures employed in our simulations can be found in Ansart et al. [53]. The
 247 frictional viscosity is omitted from each simulation with adhesion (only the
 248 frictional pressure is included) since it turns negative in the region where
 249 adhesion effect is dominant over friction effect. The drag model used is that
 250 proposed by Gobin et al. [63], which is the drag correlation of Wen and Yu
 251 [64] limited by the Ergun [65] equation for dense regimes. The gas flow is
 252 assumed to be laminar (no turbulence model is used). The agitation model
 253 used for the solid phase is $q_p^2 - q_{gp}$, which includes transport equations for the
 254 particle fluctuant kinetic energy, q_p^2 , and the gas-particle velocity covariance,
 255 q_{gp} [66, 67, 57, 68]. However, since the gas flow is assumed to be laminar,
 256 the gas fluctuating velocity $u''_{g,i}$ is zero; hence $q_{gp} = \langle u''_{g,i} u''_{p,i} \rangle_p$ equals zero.

257 Two sidewall pressure monitoring points at zero and $195d_p$ above the inlet
 258 were utilized to measure the overall bed pressure drop at each superficial gas
 259 velocity in fluidization and defluidization cycles. Each superficial gas velocity
 260 was sustained for 5 s, and the pressure was averaged over the last 2 s of each of
 261 these 5 s intervals to determine the time-averaged bed pressure drop values:

$$\overline{\Delta P} = \overline{P_1} - \overline{P_2} = \frac{1}{\sum_{k=1}^{N_r} \Delta t_k} \left(\sum_{k=1}^{N_r} \Delta t_k P_{1,k} - \sum_{k=1}^{N_r} \Delta t_k P_{2,k} \right) \quad (21)$$

263 where P_1 and P_2 are the pressures at the monitoring points, Δt is the time
 264 step, and N_r is the total number of time steps in the 2 s interval. The
 265 normalized bed pressure drop is defined as the ratio of the pressure drop
 266 across the whole bed to the pressure drop equivalent to the weight of the
 267 particles, $\overline{\Delta P} / \Delta P_{eq}$. The pressure drop ΔP_{eq} can be expressed as:

$$\Delta P_{eq} = m_b g / S_b = \alpha_p \rho_p H_b g \quad (22)$$

268 where m_b is the mass of the particles bed, g is the gravitational acceleration,
 269 S_b is the cross-sectional area of the bed, and H_b is the bed height. Substi-
 270 tuting 0.6 for α_p and $36d_p$ for H_b (see Table 2) in Eq. (22) gives ΔP_{eq} equals
 271 30.513 Pa. The spatial average of the solid volume fraction α_p is computed
 272 as follows:

$$\langle \alpha_p \rangle = \frac{1}{N_c} \sum_{i=1}^{N_c} \alpha_{p_i} \quad (23)$$

273 where N_c is the number of cells between the inlet and $34d_p$ above the inlet,
 274 which is slightly less than the bed height at the lowest superficial gas velocity.
 275 The time average of the spatially averaged α_p is determined as:

$$\overline{\langle \alpha_p \rangle} = \frac{\sum_{k=1}^{N_r} \Delta t_k \langle \alpha_p \rangle_k}{\sum_{k=1}^{N_r} \Delta t_k} \quad (24)$$

276 Then, the bed voidage is obtained as: $\overline{\langle \alpha_g \rangle} = 1 - \overline{\langle \alpha_p \rangle}$.

277 Bed pressure drop and voidage versus superficial gas velocity curves for
 278 fluidization and defluidization cycles with different B values (Eq. (19)) are
 279 shown in Fig. 2. The value of B obtained by substituting the values of A ,
 280 d_p and S_0 (given in Table 2) in Eq. (20) is 2.3×10^{-20} J. In addition to
 281 this value, we tested much higher B values in order to demonstrate that the
 282 adhesion provided by the kinetic theory model is several orders of magnitude
 283 smaller than that given by the coordination number model presented later
 284 in section 2.3. As depicted in Fig. 2, generating a pressure drop overshoot
 285 requires multiplying B by 10^6 (using $B = 2.3 \times 10^{-14}$ J) and no hysteretic
 286 behavior is predicted between the increasing and decreasing velocity path
 287 curves. The bed voidage curves displayed in Fig. 2 show a decrease in the

288 average gas volume fraction in the bed for $B = 2.3 \times 10^{-14}$ J due to the
 289 relatively strong adhesion.

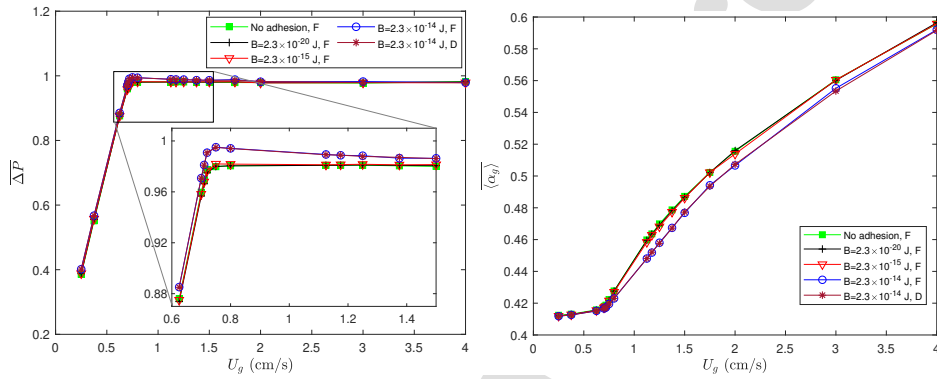


Fig. 2. Normalized time-averaged overall bed pressure drop and time-spatial averaged gas volume fraction in the bed during fluidization and defluidization cycles with different B values in the adhesion pressure (Eq. (19)). F represents a fluidization branch and D a defluidization branch in this and Fig. 4. [69].

290 Based on the foregoing results, the adhesive contribution introduced by
 291 the kinetic theory model is insufficient to generate an overshoot in the bed
 292 pressure drop. This inability might be attributed to the binary and instan-
 293 tantaneous collisions assumption used in the kinetic theory approach because
 294 fixed-bed flows are dominated by the influence of multiple and sustained
 295 contacts. The pressure-drop hysteresis between the fluidization and deflu-
 296 idization branches is not produced because the impact of deformation history
 297 is not taken into account in the kinetic theory adhesion model. In particular,
 298 the adhesive pressure is only a function of the particle volume fraction α_p ,
 299 indicating that it is a symmetric closure. In the next section, we present a
 300 coordination-number-based approach suitable for quasi-static flow regimes.

301 *2.3. Derivation of an adhesive pressure based on the coordination number*

302 Here, we derive an adhesive pressure model by assuming that the domi-
 303 nant Van der Waals interaction occurs between particles in long-lasting con-
 304 tact characterized by the coordination number. The coordination number
 305 is defined as the mean number of particles in contact with a given particle,
 306 which may be written as:

$$CN = 2 \frac{n_c}{n_p} \quad (25)$$

307 where n_c denotes the mean number of contacts per unit volume and n_p de-
 308 notes the number of particles per unit volume. The factor 2 enters in Eq. (25)
 309 because each contact is shared by two particles. The particle-particle stress
 310 tensor component due to the adhesive force may be computed as [70, 71, 72]:

311

$$\sigma_{ij}^{ad} = -\frac{1}{V} \sum_{c \in V} f_i^c b_j^c \quad (26)$$

312 where the sum is over all the contact points c in volume V . f_i^c represents the
 313 interaction force between two particles in contact at c and b_j^c represents the
 314 vector connecting the centers of these two particles if both centers are inside
 315 the volume V , or only the part in V if one of the centers is outside V . By
 316 using Eq. (5), the adhesive contact force can be expressed as follows:

$$\mathbf{F}_{p^* \rightarrow p}^c = \frac{A}{6d_p} \frac{1}{(2u_0 + u_0^2)^2} \frac{1}{(1 + u_0)^3} \mathbf{k}^* \approx \frac{A}{6d_p} \frac{1}{4u_0^2} \mathbf{k}^* \quad (27)$$

317 where $u_0 = S_0/d_p$ is the minimum dimensionless separation distance between
 318 two particle surfaces and $\mathbf{k}^* = (\mathbf{x}^* - \mathbf{x}) / \|\mathbf{x}^* - \mathbf{x}\|$ is the unit vector along the
 319 line of centers of two interacting particles. Substituting Eq. (27) into Eq.
 320 (26) gives the following adhesive stress expression for homogeneous systems:

321

$$\sigma_{ij}^{ad} = \frac{1}{V} \sum_{c \in V} \frac{A}{24u_0^2} k_i^* k_j^* \quad (28)$$

322 The isotropic component of the adhesive stress given by Eq. (28) is the
323 adhesive pressure:

$$P_p^a = -\frac{\sigma_{ii}^{ad}}{3} = -\frac{n_c}{3} \frac{Ad_p^2}{24S_0^2} \quad (29)$$

324 Then, using Eqs. (29) and (25), the adhesive particle pressure can be ex-
325 pressed as:

$$P_p^a = -\frac{\alpha_p}{\pi d_p^2} CN \frac{Ad_p}{24S_0^2} \quad (30)$$

326 where CN is the coordination number.

327 2.4. Evaluation of the coordination-number-based adhesion model

Eulerian-Eulerian simulations were carried out using the parameter values in Table 2 to check the ability of the adhesive pressure model given by Eq. (30) to create the pressure drop overshoot. These simulations are the same as those described in section 2.2, except that the coordination-number-based adhesive pressure model is utilized instead of the kinetic-theory-based one. In our tests, we used a constant coordination number of 4.77 corresponding to a fixed bed state and correlations between the coordination number and the solid volume fraction based on the CFD-DEM simulation results of Hou et al. [62]:

$$CN = 2 + 3.25\alpha_p^{0.4} \quad \text{for expanded beds} \quad (31)$$

$$CN = 4.87 \times 10^{-5} \frac{1 - (1 - \alpha_p)^{2.8}}{(1 - \alpha_p)^{11.6}} \quad \text{for fluidized beds} \quad (32)$$

328 These correlations were developed using simulations that account for the Van
329 der Waals adhesion between particles. Fig. 3 shows CN plotted as a function

330 of α_p for expanded and fluidized bed states using Eqs. (31) and (32). In the
 331 expanded bed state, as the solid volume fraction decreases from the close-
 332 packing value (0.64) to zero, the coordination number slowly decreases until
 333 it reaches a minimum value of 2 corresponding to a chain-like structure,
 334 as demonstrated in Fig. 3. On the other hand, the coordination number
 335 corresponding to the fluidized bed state decreases rapidly towards zero when
 336 the solid volume fraction decreases, as seen in Fig. 3.

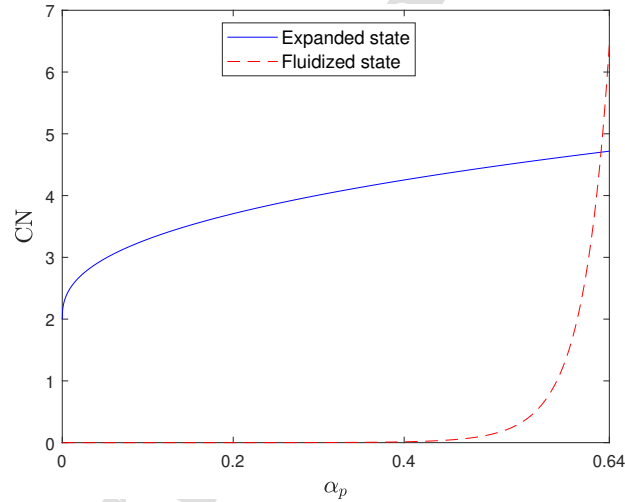


Fig. 3. CN as a function of α_p for expanded and fluidized bed states.

337 The obtained bed pressure drop and mean gas volume fraction profiles
 338 are illustrated in Fig. 4. As we can observe in the pressure drop versus
 339 superficial gas velocity plots, the constant fixed-bed coordination number and
 340 the expanded-bed correlation both generate overshoot, while the fluidized-
 341 bed correlation does not. Based on these results, we can infer that the
 342 coordination-number-based model provides an adhesive contribution large

343 enough to produce an overshoot in the bed pressure drop.

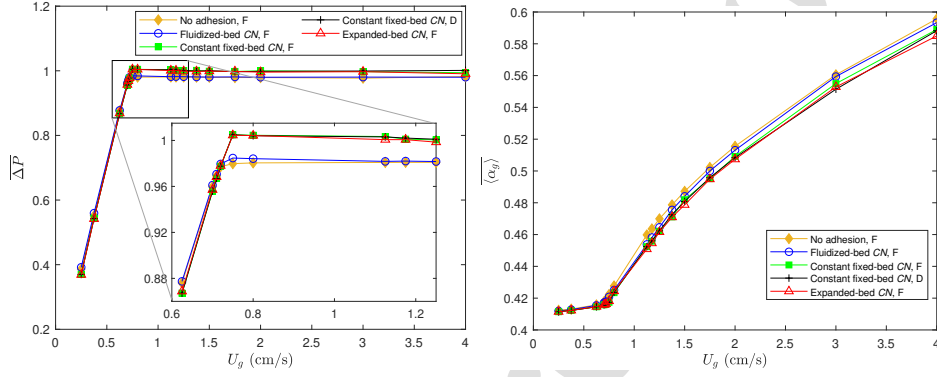


Fig. 4. Normalized time-averaged overall bed pressure drop and time-spatial averaged gas volume fraction in the bed during fluidization and defluidization cycles without and with adhesion using the coordination-number-based model. [69].

344 The experimental bed voidage curves of Geldart A particles in Fig. 1
 345 demonstrate that at superficial gas velocities less than the minimum fluidiza-
 346 tion velocity U_{mf} , the bed voidage remains constant at ε_0 in the increasing
 347 velocity path. When the superficial gas velocity reaches U_{mf} , the forces ex-
 348 erted by the gas on the particles overcome the interparticle forces, particle-
 349 wall friction, and particles' weight, leading to the destruction of the contact
 350 network and an abrupt jump in the bed voidage from ε_0 to ε_{mf} . In contrast,
 351 in the decreasing velocity path, the bed voidage progressively decreases from
 352 ε_{mf} to ε_0 as the superficial gas velocity decreases from U_{mf} to zero. The sim-
 353 ulation results in Fig. 4 show a decrease in bed voidage owing to adhesion,
 354 but the hysteretic behavior between the fluidization and defluidization cycle
 355 curves observed experimentally is not predicted. To obtain this behavior,
 356 the role of Van der Waals interparticle force and particle-wall static friction

357 should be dominant over that of hydrodynamic forces in the fixed bed state.
358 Achieving this condition is influenced by the values of the various simulation
359 model parameters. For example, the particle diameter in the experiments of
360 Soleimani et al. [14] is $67 \mu\text{m}$, which is smaller than the particle diameter in
361 our simulations ($100 \mu\text{m}$). In addition, the contact network formation and
362 destruction (the coordination number evolution) should be taken into con-
363 sideration in our two-fluid simulations to generate the hysteresis. Moreover,
364 the effect of boundary conditions (particle-wall friction) and dimensionality
365 (quasi-2D to 3D) on the pressure overshoot should be explored. Consider-
366 ing the effect of static particle-wall friction on the pressure-drop overshoot
367 in the two-fluid model could be the subject of future research. Accounting
368 for this effect is essential to achieve a quantitative prediction because static
369 wall friction may increase the overshoot intensity. However, the significance
370 of this impact depends on the column diameter [32]. Regarding the effect
371 of particle size, our simulations using the coordination-number-based model
372 demonstrated that the diminution of the particle diameter notably increases
373 the pressure overshoot intensity (data not shown here), which is consistent
374 with experimental observations [15].

375 The number of interparticle contacts, and hence the radial distribution
376 function, is influenced by adhesion. This could be investigated through DEM
377 simulations. In the fixed-bed state, the dominant effect is for the frictional
378 pressure and not the collisional pressure. Therefore, modifying the radial
379 distribution function to consider the influence of adhesion may have a negli-
380 gible effect on the overshoot obtained using the coordination number model.
381 The kinetic theory adhesion model gives an adhesive contribution 6 orders

382 of magnitude smaller than that of the coordination number model. This is
383 because the kinetic theory assumptions, including the assumption that the
384 radial distribution function is not modified by adhesion, are not valid.

385 **3. Conclusion**

386 In this research, two-fluid model simulations were performed with the
387 aim of predicting the pressure-drop overshoot observed during fluidization of
388 Geldart A particles. Two adhesive pressure models were suggested to account
389 for the Van der Waals force among particles. The first model, which is based
390 on the kinetic theory, gives an adhesion effect that is not strong enough to
391 create the pressure drop overshoot. This model may be suitable for rapid
392 granular flows, but it is not appropriate for quasi-static flows because it does
393 not account for the long term and multiple particle-particle contacts. The
394 second model, which is expressed in terms of the mean number of contacts per
395 particle, makes use of CFD-DEM correlations that relate the coordination
396 number to the solid volume fraction for various flow conditions. This model
397 gives an adhesive contribution far larger than the one of the kinetic theory
398 model and produces the overshoot in the bed pressure drop. The success
399 of the aforementioned model appears to be attributable to the fact that it
400 accounts for the multiple and sustained contacts. The hysteresis between the
401 fluidization and defluidization branches was not predicted by any of the two
402 adhesive pressure models.

403 A meso-scale numerical investigation is required to guide postulating a
404 continuum evolution equation for the coordination number or developing an
405 Eulerian adhesive stress closure that accounts for the effect of deformation

406 history and the transition between the different flow regimes (fixed, expanded
407 and fluidized bed states) in order to predict the hysteresis in the bed pressure
408 drop at the macro-scale.

409 Some researchers have previously claimed that the standard two-fluid
410 model, which does not account for adhesion between particles, can correctly
411 predict the fluidization behavior of Geldart A particles if a sufficiently high
412 resolution is used. For example, Wang et al. [73] demonstrated that fluidized
413 bed expansion can be accurately predicted (compared to discrete particle
414 simulations) when the cell size is of the order of three particle diameters
415 and the time step is small. However, they only studied the bed expansion
416 at superficial gas velocities well above the minimum fluidization velocity, at
417 which the coordination number and hence the adhesive contribution may be
418 negligible. Our two-fluid simulations employ a small time step and a cell size
419 of two times the particle diameter, which complies with the recommendation
420 of Wang et al. [73]. The results of these simulations reveal that no over-
421 shoot is generated during the transition from fixed to fluidized bed without
422 considering the effects of adhesion. Therefore, interparticle attractive forces
423 may have a significant contribution to the hydrodynamic behavior observed
424 in fluidized-bed experiments. Taking these adhesive interactions into account
425 is critical for gaining a comprehensive understanding of the fluidization be-
426 havior of particles belonging to Geldart group A.

427 **Acknowledgments**

428 This project was provided with computing and storage resources by GENCI
429 on the CSL/SKL partition of the Jean-Zay/Joliot-Curie supercomputer at

430 IDRIS/TGCC thanks to grant A0142B06938, and by CALMIP through grant
431 P1132.

432 References

- 433 [1] D. Kunii, O. Levenspiel, Fluidization engineering, Butterworth-
434 Heinemann, 1991.
435 URL <https://books.google.ca/books?id=ZVnb17qRz8QC>
- 436 [2] W.-c. Yang, Handbook of fluidization and fluid-particle systems, CRC
437 press, 2003.
438 URL <https://books.google.ca/books?id=lHTUphHZyogC>
- 439 [3] J. R. Grace, J. Chaouki, T. Pugsley, Fluidized bed reactor, Particle
440 Technology and Applications (2012) 199.
441 URL <https://doi.org/10.1201/b11904>
- 442 [4] J. Shabaniyan, J. Chaouki, Effects of temperature, pressure, and interpar-
443 ticle forces on the hydrodynamics of a gas-solid fluidized bed, Chemical
444 Engineering Journal 313 (2017) 580–590.
445 URL <https://doi.org/10.1016/j.cej.2016.12.061>
- 446 [5] P. Lettieri, D. Macrì, Effect of process conditions on fluidization, KONA
447 Powder and Particle Journal 33 (2016) 86–108.
448 URL <https://doi.org/10.14356/kona.2016017>
- 449 [6] J. Shabaniyan, R. Jafari, J. Chaouki, Fluidization of ultrafine powders,
450 International review of chemical engineering 4 (1) (2012) 16–50.

- 451 [7] J. Ma, J. R. van Ommen, D. Liu, R. F. Mudde, X. Chen, S. Pan,
452 C. Liang, Fluidization dynamics of cohesive geldart b particles. part ii:
453 Pressure fluctuation analysis, *Chemical Engineering Journal* 368 (2019)
454 627–638.
455 URL <https://doi.org/10.1016/j.cej.2019.02.187>
- 456 [8] G. Hendrickson, Electrostatics and gas phase fluidized bed polymeriza-
457 tion reactor wall sheeting, *Chemical Engineering Science* 61 (4) (2006)
458 1041–1064.
459 URL <https://doi.org/10.1016/j.ces.2005.07.029>
- 460 [9] P. Rajniak, C. Mancinelli, R. Chern, F. Stepanek, L. Farber, B. Hill,
461 Experimental study of wet granulation in fluidized bed: Impact of the
462 binder properties on the granule morphology, *International journal of*
463 *pharmaceutics* 334 (1-2) (2007) 92–102.
464 URL <https://doi.org/10.1016/j.ijpharm.2006.10.040>
- 465 [10] B. J. Skrifvars, M. Hupa, M. Hiltunen, Sintering of ash during fluidized
466 bed combustion, *Industrial & engineering chemistry research* 31 (4)
467 (1992) 1026–1030.
468 URL <https://pubs.acs.org/doi/pdf/10.1021/ie00004a008>
- 469 [11] P. Jiang, H. Bi, S.-C. Liang, L.-S. Fan, Hydrodynamic behavior of cir-
470 culating fluidized bed with polymeric particles, *AIChE Journal* 40 (2)
471 (1994) 193–206.
472 URL <https://doi.org/10.1002/aic.690400202>
- 473 [12] J. Shabaniyan, J. Chaouki, Hydrodynamics of a gas–solid fluidized bed

- 474 with thermally induced interparticle forces, Chemical Engineering Jour-
475 nal 259 (2015) 135–152.
476 URL <https://doi.org/10.1016/j.cej.2014.07.117>
- 477 [13] E. Jaraiz, S. Kimura, O. Levenspiel, Vibrating beds of fine particles:
478 estimation of interparticle forces from expansion and pressure drop ex-
479 periments, Powder technology 72 (1) (1992) 23–30.
480 URL [https://doi.org/10.1016/S0032-5910\(92\)85017-P](https://doi.org/10.1016/S0032-5910(92)85017-P)
- 481 [14] I. Soleimani, N. Elahipanah, J. Shabaniyan, J. Chaouki, In-situ quan-
482 tification of the magnitude of interparticle forces and its temperature
483 variation in a gas-solid fluidized bed, Chemical Engineering Science 232
484 (2021) 116349.
485 URL <https://doi.org/10.1016/j.ces.2020.116349>
- 486 [15] S. Affleck, A. Thomas, A. Routh, N. Vriend, Novel protocol for quanti-
487 fying powder cohesivity through fluidisation tests, Powder Technology
488 415 (2023) 118147.
489 URL <https://doi.org/10.1016/j.powtec.2022.118147>
- 490 [16] J. Visser, Van der waals and other cohesive forces affecting powder flu-
491 idization, Powder Technology 58 (1) (1989) 1–10.
492 URL [https://doi.org/10.1016/0032-5910\(89\)80001-4](https://doi.org/10.1016/0032-5910(89)80001-4)
- 493 [17] J. N. Israelachvili, Intermolecular and surface forces, Academic press,
494 2011.
495 URL <https://books.google.ca/books?id=vgyBJbtN0coC>

- 496 [18] H. C. Hamaker, The london—van der waals attraction between spherical
497 particles, *physica* 4 (10) (1937) 1058–1072.
498 URL [https://doi.org/10.1016/S0031-8914\(37\)80203-7](https://doi.org/10.1016/S0031-8914(37)80203-7)
- 499 [19] F. London, The general theory of molecular forces, *Transactions of the*
500 *Faraday Society* 33 (1937) 8b–26.
501 URL <https://doi.org/10.1039/TF937330008B>
- 502 [20] C. Q. LaMarche, S. Leadley, P. Liu, K. M. Kellogg, C. M. Hrenya,
503 Method of quantifying surface roughness for accurate adhesive force pre-
504 dictions, *Chemical Engineering Science* 158 (2017) 140–153.
505 URL <https://doi.org/10.1016/j.ces.2016.09.024>
- 506 [21] Q. Li, V. Rudolph, W. Peukert, London-van der waals adhesiveness of
507 rough particles, *Powder Technology* 161 (3) (2006) 248–255.
508 URL <https://doi.org/10.1016/j.powtec.2005.10.012>
- 509 [22] H. Krupp, Particle adhesion theory and experiment, *Advan. Colloid*
510 *Interface Sci.* 1 (1967) 111–239.
511 URL [https://doi.org/10.1016/0001-8686\(67\)80004-6](https://doi.org/10.1016/0001-8686(67)80004-6)
- 512 [23] B. Formisani, R. Girimonte, L. Mancuso, Analysis of the fluidization
513 process of particle beds at high temperature, *Chemical Engineering Sci-*
514 *ence* 53 (5) (1998) 951–961.
515 URL [https://doi.org/10.1016/S0009-2509\(97\)00370-9](https://doi.org/10.1016/S0009-2509(97)00370-9)
- 516 [24] J. Shabanian, J. Chaouki, Fluidization characteristics of a bubbling gas–
517 solid fluidized bed at high temperature in the presence of interparticle

- 518 forces, *Chemical Engineering Journal* 288 (2016) 344–358.
519 URL <https://doi.org/10.1016/j.cej.2015.12.016>
- 520 [25] H. Piepers, E. J. E. Cottaar, A. Verkooijen, K. Rietema, Effects of pres-
521 sure and type of gas on particle-particle interaction and the consequences
522 for gas—solid fluidization behaviour, *Powder Technology* 37 (1) (1984)
523 55–70.
524 URL [https://doi.org/10.1016/0032-5910\(84\)80006-6](https://doi.org/10.1016/0032-5910(84)80006-6)
- 525 [26] H.-Y. Xie, The role of interparticle forces in the fluidization of fine par-
526 ticles, *Powder Technology* 94 (2) (1997) 99–108.
527 URL [https://doi.org/10.1016/S0032-5910\(97\)03270-1](https://doi.org/10.1016/S0032-5910(97)03270-1)
- 528 [27] A. Srivastava, S. Sundaresan, Role of wall friction in fluidization and
529 standpipe flow, *Powder technology* 124 (1-2) (2002) 45–54.
530 URL [https://doi.org/10.1016/S0032-5910\(01\)00471-5](https://doi.org/10.1016/S0032-5910(01)00471-5)
- 531 [28] S. Mutsers, K. Rietema, The effect of interparticle forces on the ex-
532 pansion of a homogeneous gas-fluidized bed, *Powder Technology* 18 (2)
533 (1977) 239–248.
534 URL [https://doi.org/10.1016/0032-5910\(77\)80014-4](https://doi.org/10.1016/0032-5910(77)80014-4)
- 535 [29] S. Tsinontides, R. Jackson, The mechanics of gas fluidized beds with
536 an interval of stable fluidization, *Journal of Fluid Mechanics* 255 (1993)
537 237–274.
538 URL <https://doi.org/10.1017/S0022112093002472>
- 539 [30] K. Rietema, H. Piepers, The effect of interparticle forces on the stability
540 of gas-fluidized beds—i. experimental evidence, *Chemical Engineering*

- 541 Science 45 (6) (1990) 1627–1639.
542 URL [https://doi.org/10.1016/0009-2509\(90\)80015-7](https://doi.org/10.1016/0009-2509(90)80015-7)
- 543 [31] B. Liu, X. Zhang, L. Wang, H. Hong, Fluidization of non-spherical par-
544 ticles: Sphericity, zingg factor and other fluidization parameters, Partic-
545 uology 6 (2) (2008) 125–129.
546 URL <https://doi.org/10.1016/j.cpart.2007.07.005>
- 547 [32] F. Vanni, B. Caussat, C. Ablitzer, M. Brothier, Effects of reducing the
548 reactor diameter on the fluidization of a very dense powder, Powder
549 Technology 277 (2015) 268–274.
550 URL <https://doi.org/10.1016/j.powtec.2015.03.010>
- 551 [33] S. Sánchez-Delgado, J. A. Almendros-Ibáñez, N. García-Hernando,
552 D. Santana, On the minimum fluidization velocity in 2d fluidized beds,
553 Powder Technology 207 (1-3) (2011) 145–153.
554 URL <https://doi.org/10.1016/j.powtec.2010.10.020>
- 555 [34] H. Matuttis, S. Luding, H. Herrmann, Discrete element simulations of
556 dense packings and heaps made of spherical and non-spherical particles,
557 Powder technology 109 (1-3) (2000) 278–292.
558 URL [https://doi.org/10.1016/S0032-5910\(99\)00243-0](https://doi.org/10.1016/S0032-5910(99)00243-0)
- 559 [35] X. S. Wang, F. Rahman, M. J. Rhodes, Nanoparticle fluidization and
560 geldart's classification, Chemical Engineering Science 62 (13) (2007)
561 3455–3461.
562 URL <https://doi.org/10.1016/j.ces.2007.02.051>

- 563 [36] J. W. Landry, G. S. Grest, L. E. Silbert, S. J. Plimpton, Confined gran-
564 ular packings: structure, stress, and forces, *Physical review E* 67 (4)
565 (2003) 041303.
566 URL <https://doi.org/10.1103/PhysRevE.67.041303>
- 567 [37] J. W. Landry, G. S. Grest, S. J. Plimpton, Discrete element simulations
568 of stress distributions in silos: crossover from two to three dimensions,
569 *Powder technology* 139 (3) (2004) 233–239.
570 URL <https://doi.org/10.1016/j.powtec.2003.10.016>
- 571 [38] C. A. Ho, M. Sommerfeld, Modelling of micro-particle agglomeration
572 in turbulent flows, *Chemical Engineering Science* 57 (15) (2002) 3073–
573 3084.
574 URL [https://doi.org/10.1016/S0009-2509\(02\)00172-0](https://doi.org/10.1016/S0009-2509(02)00172-0)
- 575 [39] S. Wang, H. Lu, Z. Shen, H. Liu, J. Bouillard, Prediction of flow behav-
576 ior of micro-particles in risers in the presence of van der waals forces,
577 *Chemical Engineering Journal* 132 (1-3) (2007) 137–149.
578 URL <https://doi.org/10.1016/j.cej.2007.01.043>
- 579 [40] M. Zhang, K. Chu, F. Wei, A. Yu, A cfd–dem study of the cluster
580 behavior in riser and downer reactors, *Powder Technology* 184 (2) (2008)
581 151–165.
582 URL <https://doi.org/10.1016/j.powtec.2007.11.036>
- 583 [41] D. Gidaspow, L. Huilin, Equation of state and radial distribution func-
584 tions of fcc particles in a cfb, *AIChE Journal* 44 (2) (1998) 279–293.
585 URL <https://doi.org/10.1002/aic.690440207>

- 586 [42] J.-F. Parmentier, Extension of the euler/euler formalism for numerical
587 simulations of fluidized beds of geldart a particles, Ph.D. thesis, Institut
588 National Polytechnique de Toulouse, thesis directed by Olivier Simonin
589 (2010).
590 URL <http://www.theses.fr/2010INPT0121/document>
- 591 [43] J. T. Jenkins, D. Berzi, Dense inclined flows of inelastic spheres: tests of
592 an extension of kinetic theory, *Granular Matter* 12 (2) (2010) 151–158.
593 URL <https://doi.org/10.1007/s10035-010-0169-8>
- 594 [44] S. Chialvo, J. Sun, S. Sundaresan, Bridging the rheology of granular
595 flows in three regimes, *Physical review E* 85 (2) (2012) 021305.
596 URL <https://doi.org/10.1103/PhysRevE.85.021305>
- 597 [45] S. Schneiderbauer, A. Aigner, S. Pirker, A comprehensive frictional-
598 kinetic model for gas–particle flows: Analysis of fluidized and moving
599 bed regimes, *Chemical Engineering Science* 80 (2012) 279–292.
600 URL <https://doi.org/10.1016/j.ces.2012.06.041>
- 601 [46] P. N. Loezos, P. Costamagna, S. Sundaresan, The role of contact stresses
602 and wall friction on fluidization, *Chemical Engineering Science* 57 (24)
603 (2002) 5123–5141.
604 URL [https://doi.org/10.1016/S0009-2509\(02\)00421-9](https://doi.org/10.1016/S0009-2509(02)00421-9)
- 605 [47] M. Ye, M. A. van der Hoef, J. Kuipers, The effects of particle and gas
606 properties on the fluidization of geldart a particles, *Chemical engineering
607 science* 60 (16) (2005) 4567–4580.
608 URL <https://doi.org/10.1016/j.ces.2005.03.017>

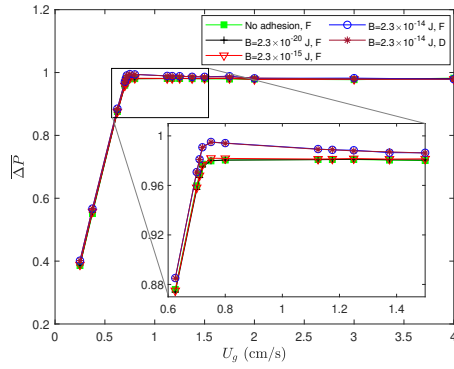
- 609 [48] M. W. Weber, C. M. Hrenya, Computational study of pressure-drop
610 hysteresis in fluidized beds, *Powder technology* 177 (3) (2007) 170–184.
611 URL <https://doi.org/10.1016/j.powtec.2007.01.016>
- 612 [49] M. Askarishahi, M.-S. Salehi, S. Radl, Capability of the tfm approach
613 to predict fluidization of cohesive powders, *Industrial & Engineering*
614 *Chemistry Research* 61 (8) (2022) 3186–3205.
615 URL <https://doi.org/10.1021/acs.iecr.1c04786>
- 616 [50] Y. Gu, A. Ozel, J. Kolehmainen, S. Sundaresan, Computationally gen-
617 erated constitutive models for particle phase rheology in gas-fluidized
618 suspensions, *Journal of Fluid Mechanics* 860 (2019) 318–349.
619 URL <https://doi.org/10.1017/jfm.2018.856>
- 620 [51] Y. Wu, Q. Hou, A. Yu, Linking discrete particle simulation to continuum
621 properties of the gas fluidization of cohesive particles, *AICHE Journal*
622 66 (5) (2020) e16944.
623 URL <https://doi.org/10.1002/aic.16944>
- 624 [52] H. Neau, M. Pigou, P. Fede, R. Ansart, C. Baudry, N. Mériçoux,
625 J. Laviéville, Y. Fournier, N. Renon, O. Simonin, Massively parallel
626 numerical simulation using up to 36,000 cpu cores of an industrial-scale
627 polydispersed reactive pressurized fluidized bed with a mesh of one bil-
628 lion cells, *Powder Technology* 366 (2020) 906–924.
629 URL <https://doi.org/10.1016/j.powtec.2020.03.010>
- 630 [53] R. Ansart, P. García-Triñanes, B. Boissière, H. Benoit, J. P. Seville,
631 O. Simonin, Dense gas-particle suspension upward flow used as heat

- 632 transfer fluid in solar receiver: Pept experiments and 3d numerical sim-
633 ulations, Powder Technology 307 (2017) 25–36.
634 URL <https://doi.org/10.1016/j.powtec.2016.11.006>
- 635 [54] B. Van Wachem, S. Sasic, Derivation, simulation and validation of a
636 cohesive particle flow cfd model, AIChE Journal 54 (1) (2008) 9–19.
637 URL <https://doi.org/10.1002/aic.11335>
- 638 [55] P. C. Johnson, P. Nott, R. Jackson, Frictional–collisional equations of
639 motion for particulate flows and their application to chutes, Journal of
640 fluid mechanics 210 (1990) 501–535.
641 URL <https://doi.org/10.1017/S0022112090001380>
- 642 [56] A. Srivastava, S. Sundaresan, Analysis of a frictional–kinetic model for
643 gas–particle flow, Powder technology 129 (1-3) (2003) 72–85.
644 URL [https://doi.org/10.1016/S0032-5910\(02\)00132-8](https://doi.org/10.1016/S0032-5910(02)00132-8)
- 645 [57] O. Simonin, Statistical and continuum modelling of turbulent reactive
646 particulate flows, Lecture series 6 (2000).
- 647 [58] X. He, G. D. Doolen, Thermodynamic foundations of kinetic theory and
648 lattice boltzmann models for multiphase flows, Journal of Statistical
649 Physics 107 (1) (2002) 309–328.
650 URL <https://doi.org/10.1023/A:1014527108336>
- 651 [59] M. Elimelech, J. Gregory, X. Jia, R. Williams, Particle Deposition and
652 Aggregation: Measurement, Modelling and Simulation, Elsevier Science,
653 2013.
654 URL <https://books.google.ca/books?id=R6g3BQAAQBAJ>

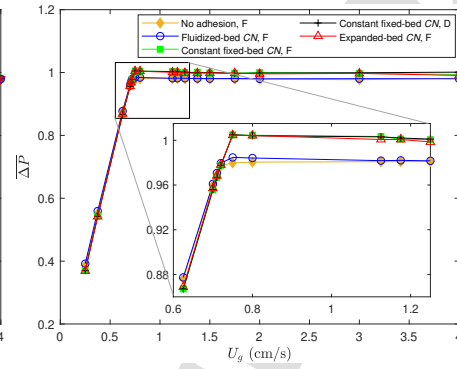
- 655 [60] R. Yang, R. Zou, A. Yu, Computer simulation of the packing of fine
656 particles, *Physical review E* 62 (3) (2000) 3900.
657 URL <https://doi.org/10.1103/PhysRevE.62.3900>
- 658 [61] C. Lun, S. Savage, The effects of an impact velocity dependent coefficient
659 of restitution on stresses developed by sheared granular materials, *Acta*
660 *Mechanica* 63 (1) (1986) 15–44.
661 URL <https://doi.org/10.1007/BF01182538>
- 662 [62] Q. Hou, Z. Zhou, A. Yu, Micromechanical modeling and analysis of
663 different flow regimes in gas fluidization, *Chemical Engineering Science*
664 84 (2012) 449–468.
665 URL <https://doi.org/10.1016/j.ces.2012.08.051>
- 666 [63] A. Gobin, H. Neau, O. Simonin, J.-R. Llinas, V. Reiling, J.-L. Sélo, Fluid
667 dynamic numerical simulation of a gas phase polymerization reactor,
668 *International journal for numerical methods in fluids* 43 (10-11) (2003)
669 1199–1220.
670 URL <https://doi.org/10.1002/flid.542>
- 671 [64] C. Wen, Y. Yu, Mechanics of fluidization, in: *Chem. Eng. Prog. Symp.*
672 *Ser.*, Vol. 62, 1966, pp. 100–111.
673 URL <https://cir.nii.ac.jp/crid/1572261550060180736>
- 674 [65] S. Ergun, Fluid flow through packed columns, *Chem. Eng. Prog.* 48 (2)
675 (1952) 89–94.
676 URL <https://cir.nii.ac.jp/crid/1572543025220678016>

- 677 [66] O. Simonin, E. Deutsch, J. Minier, Eulerian prediction of the
678 fluid/particle correlated motion in turbulent two-phase flows, Applied
679 Scientific Research 51 (1993) 275–283.
680 URL <https://doi.org/10.1007/BF01082549>
- 681 [67] P. Fevrier, O. Simonin, Constitutive relations for fluid-particle velocity
682 correlations in gas-solid turbulent flows, in: Third International Confer-
683 ence on Multiphase Flows, ICMF, Vol. 98, 1998, pp. 8–12.
- 684 [68] F. Fotovat, R. Ansart, M. Hemati, O. Simonin, J. Chaouki, Sand-
685 assisted fluidization of large cylindrical and spherical biomass particles:
686 Experiments and simulation, Chemical Engineering Science 126 (2015)
687 543–559.
688 URL <https://doi.org/10.1016/j.ces.2014.12.022>
- 689 [69] Y. Badran, R. Ansart, J. Chaouki, O. Simonin, Effect of van der waals
690 force on fluidization of fine particles, in: 13th International Conference
691 on Fluidized Bed Technology (CFB-13), Vancouver, Canada, 2021, pp.
692 124–129.
- 693 [70] C. Goldenberg, A. P. Atman, P. Claudin, G. Combe, I. Goldhirsch,
694 Scale separation in granular packings: stress plateaus and fluctuations,
695 Physical review letters 96 (16) (2006) 168001.
696 URL <https://doi.org/10.1103/PhysRevLett.96.168001>
- 697 [71] J. Zhang, T. Majmudar, A. Tordesillas, R. Behringer, Statistical proper-
698 ties of a 2d granular material subjected to cyclic shear, Granular Matter

- 699 12 (2010) 159–172.
700 URL <https://doi.org/10.1007/s10035-010-0170-2>
- 701 [72] S. Luding, Anisotropy in cohesive, frictional granular media, *Journal of*
702 *Physics: Condensed Matter* 17 (24) (2005) S2623.
703 URL <https://dx.doi.org/10.1088/0953-8984/17/24/017>
- 704 [73] J. Wang, M. A. van der Hoef, J. Kuipers, Why the two-fluid model fails
705 to predict the bed expansion characteristics of geldart a particles in gas-
706 fluidized beds: a tentative answer, *Chemical Engineering Science* 64 (3)
707 (2009) 622–625.
708 URL <https://doi.org/10.1016/j.ces.2008.09.028>



(a) Kinetic-theory-based adhesion model



(b) Coordination-number-based adhesion model

Highlights

- Two adhesion pressure closures are given for the Van der Waals force effect in TFM.
- The kinetic theory fails to predict a pressure overshoot in a fluidized bed.
- The coordination number model is successful in generating the pressure overshoot.
- Interparticle Van der Waals force contributes to the pressure overshoot phenomenon.

Declaration of interests

The authors declare that they have no known competing financial interests or personal relationships that could have appeared to influence the work reported in this paper.

The authors declare the following financial interests/personal relationships which may be considered as potential competing interests:

Journal Pre-proof